Rashba spin-orbit interaction in graphene and zigzag nanoribbons

Mahdi Zarea and Nancy Sandler
Department of Physics and Astronomy, Nanoscale and Quantum Phenomena Institute, and Condensed Matter and Surface Science Program, Ohio University, Athens, Ohio 45701-2979, USA

(Received 31 December 2008; revised manuscript received 4 March 2009; published 30 April 2009)

We investigate the effects of Rashba spin-orbit (RSO) interactions on the electronic band structure and corresponding wave functions of graphene. By exactly solving a tight-binding model Hamiltonian we obtain the expected splitting of the bands—due to the SU(2) spin symmetry breaking—that is accompanied by the appearance of additional Dirac points. These points are originated by valence-conduction-band crossings. By introducing a convenient gauge transformation we study a model for zigzag nanoribbons with RSO interactions. We show that RSO interactions lift the quasidegeneracy of the edge band while introducing a state-dependent spin separation in real space. Calculation of the average magnetization perpendicular to the ribbon plane suggest that RSO could be used to produce spin-polarized currents. Comparisons with the intrinsic spin-orbit interaction proposed to exist in graphene are also presented.

DOI: 10.1103/PhysRevB.79.165442 PACS number(s): 73.20.At, 85.75.−d, 73.63.Bd, 81.05.Uw

I. INTRODUCTION

Understanding the mechanism for the generation and manipulation of spin-polarized currents is one of the greatest challenges for the development of spin-based devices. Much of the advance in the field in latest years[1] has been achieved by studying semiconductor materials which make up the bulk of current electronic circuitry. Among the mechanisms proposed to induce spin-polarized currents, the spin Hall effect (SHE) appears as the most efficient one. The SHE refers to the phenomenon in which a spin-polarized current is created when an external bias voltage is applied to the system. The effect is based on a coupling between spin and momentum degrees of freedom, and usually the existence of some kind of spin-orbit (SO) interaction in the particular system under study is invoked. For bulk semiconductor materials, for example, the SO interaction has been proposed to lead to two different manifestations of SHE: (a) the *intrinsic* SHE,[2,3] in which the material inherits a strong SO interaction from its atomic constituents or due to its crystalline symmetries (lack of inversion symmetry) and (b) the *extrinsic* SHE,[4,5] in which spin-polarized currents appear as a consequence of electron scattering by a SO-dependent scattering potential. In this last situation the scattering potential may be caused, for instance, by magnetic impurities that couple via a spin-orbit term to the conducting electrons or by defects that produce spin-dependent scattering. Among these scenarios one possibility is when interfaces or surfaces are considered. In this case, the existence of the interface/surface introduces inversion symmetry breaking and, thus, materials that do not fall into the categories cited above can also exhibit SHE. The effective SO interaction generated in this situation is known as the Rashba spin-orbit (RSO) interaction responsible for the Rashba effect.[6] Among the many materials in which RSO interactions could be exploited to obtain spin-polarized currents, graphene presents a unique and intriguing case. The material, first isolated as a single layer of graphite in 2004,[7] gives access to a crystalline surface with linear dispersion around two independent points in its Brillouin zone, the Dirac points. The special dispersion plus its crystal structure (two-atom base triangular lattice) makes possible to calculate low-energy properties using Dirac-type models as the vast literature in recent years shows.[8] Furthermore, the two sublattices of the honeycomb structure makes appropriate the use of two-valued wave functions, or spinors, for calculations of various properties. The relativistic description for low-energy properties has also been used to argue for the relevance of additional terms in the standard Dirac Hamiltonian, including an intrinsic spin-orbit (I-SO) interaction represented by a second-neighbor spin-dependent hopping term that respects all the symmetries of the graphene plane.[9] One of the consequences of this I-SO interaction is to make possible the existence of spin-polarized edge states in a new phase of matter, the quantum spin Hall (QSH) phase.[10] In previous works we have studied the physics introduced by this interaction in narrow graphene ribbons with armchair and zigzag edge terminations and in the presence of electron-electron interactions.[11,12] We have shown that the I-SO interaction does not change the metallic behavior of armchair nanoribbons in contrast with the predicted result for graphene sheets. Moreover, the interaction produces spin-filtered states localized along the edges of the ribbon, (independent of edge termination) and, as a consequence, the current induced by an applied low external voltage is spin polarized. These results are in good agreement with several numerical and analytic studies[13–22] that point to various magnetic instabilities that graphene ribbons may sustain, leading to some kind of magnetic order along the edges. Unfortunately, all numerical estimates for the strength of the I-SO interaction remain, although still controversial, rather small, in the range of 0.05–0.0011 meV (600–13 mK).[23]

However, as a pure two-dimensional material, a graphene flake on a substrate lacks inversion symmetry and it is natural to expect that a RSO interaction may introduce important changes to the material properties. The RSO coupling λ_R is controlled by the applied bias and although predicted to be in the range of $\lambda_R \sim 1$ meV (Refs. 24–26) recent experiments have shown that it can reach values up to $\lambda_R \sim 200$ meV for graphene deposited on a Ni substrate.[27] Furthermore, experiments also have shown short spin-relaxation times that sug-

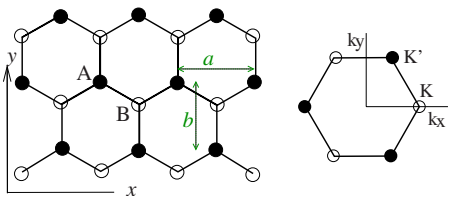

FIG. 1. (Color online) Left panel: graphene lattice. Lengths along the x and y directions are measured in units of a and $b=a\sqrt{3}/2$, respectively. Right panel: First Brillouin zone. $K=(4\pi/3a,0)$ and $K'=(2\pi/3a,\pi/b)$ are Dirac points.

gest an important effect of spin-orbit interactions in graphene.[28–31]

These developments highlight the need for a better understanding of the role played by the RSO interaction on various properties of graphene and graphene ribbons. In this work we address the questions raised by the presence of RSO in graphene sheets and zigzag ribbons. The RSO interaction strongly affects the dispersion relation near the two independent Dirac points as well as the nature of the corresponding wave functions as we will show below. As a SU(2) breaking symmetry interaction, it favors a spatial spin ordering but in contrast to the I-SO interaction introduced above, the spin order is not originated on each individual state having the same spatial spin distribution but it emerges from averaging over several states.

II. GRAPHENE SHEET: MODEL

To describe a graphene sheet (an infinite monolayer of carbon atoms arranged in a honeycomb structure), we introduce, as usual, two sublattices A and B with their respective atoms connected by vectors

$$\boldsymbol{\delta}_1 = a(0,1/\sqrt{3}),$$

$$\boldsymbol{\delta}_2 = a(1/2,-1/2\sqrt{3}),$$

$$\boldsymbol{\delta}_3 = a(-1/2,-1/2\sqrt{3}), \tag{1}$$

where $a=2.4$ Å is the lattice constant [see Fig. 1].

In the absence of SO interactions spin-up and spin-down electrons are degenerate. The SU(2) symmetric Hamiltonian and four-component spinor wave-function in momentum space are given by

$$H=\begin{pmatrix} 0 & \varphi & 0 & 0 \\ \bar{\varphi} & 0 & 0 & 0 \\ 0 & 0 & 0 & \varphi \\ 0 & 0 & \bar{\varphi} & 0 \end{pmatrix} \quad \Psi=\begin{pmatrix} u_{A\uparrow} \\ u_{B\uparrow} \\ u_{A\downarrow} \\ u_{B\downarrow} \end{pmatrix} \tag{2}$$

with $\varphi(k_x,k_y)=t(e^{ik_y 2b/3}+2\cos\frac{k_x a}{2}e^{-ik_y b/3})$. In these expressions $\bar{\varphi}$ is defined as $\bar{\varphi}(k_x,k_y)=\varphi(k_x,-k_y)$. Notice that for real values of k_y, $\bar{\varphi}=\varphi^*$. The eigenvalues of Eq. (2) are $E=\pm\varepsilon=\pm\sqrt{\varphi\bar{\varphi}}$ and the corresponding eigenvectors are defined in terms of the angle α_0 as

$$\Psi_{\pm\uparrow}=N\begin{pmatrix} e^{i\alpha_0/2} \\ \pm e^{-i\alpha_0/2} \\ 0 \\ 0 \end{pmatrix} e^{ik_x x}e^{ik_y y}, \tag{3}$$

$$\Psi_{\pm\downarrow}=N\begin{pmatrix} 0 \\ 0 \\ e^{i\alpha_0/2} \\ \pm e^{-i\alpha_0/2} \end{pmatrix} e^{ik_x x}e^{ik_y y}, \tag{4}$$

with $\varphi=|\varphi|e^{i\alpha_0}$ and N the normalization factor. For neutral graphene, $\Psi_+(\Psi_-)$ represents solutions with $E>0(E<0)$ and refers to electron (hole) conduction (valence) bands. In this language, the particle-hole symmetry implies that for each electron state with energy $E=\varepsilon$ and eigenstate characterized by α_0, there is a hole state with $E=-\varepsilon$ and eigenstate given by $\alpha_0+\pi$.

A. Rashba spin-orbit interaction

Depositing graphene on substrates and/or applying external fields makes possible to introduce a controllable RSO interaction. In the following we take the effective electric field $\mathcal{E}$ perpendicular to the graphene plane.[10,32,33] The Rashba Hamiltonian is then given by

$$H_R=\sum_{\langle ij\rangle} ic_i^\dagger(\vec{u}_{ij}\cdot\sigma)c_j+\text{H.c.}, \tag{5}$$

where σ represents the Pauli-spin operator for the spin degree of freedom. Here $\vec{u}_{ij}$ is given by

$$\vec{u}_{ij}=\frac{e}{2m^2 dv_F}\vec{\mathcal{E}}\times\vec{\delta}_{ij}=-\frac{\lambda_R}{d}\hat{z}\times\vec{\delta}_{ij}., \tag{6}$$

where $\vec{\mathcal{E}}$ is the applied electric field in the direction perpendicular to the graphene sheet, $d=a/\sqrt{3}$ is the distance between the two adjacent sites (i,j), and $\vec{\delta}_{ij}=\boldsymbol{\delta}_j-\boldsymbol{\delta}_i$ is a vector on the graphene plane.

With these definitions the RSO interaction takes the form

$$H_R=ic_{A\alpha}^\dagger R^{\alpha\beta}c_{B\beta}+\text{H.c.}, \tag{7}$$

where

$$R^{\xi\eta}=[e^{ik_y d}\sigma_x^{\xi\eta}+e^{ik_x d\sqrt{3}/2-ik_y d/2}(-\sigma_x^{\xi\eta}/2-\sigma_y^{\xi\eta}\sqrt{3}/2) + e^{-ik_x d\sqrt{3}/2-ik_y d/2}(-\sigma_x^{\xi\eta}/2+\sigma_y^{\xi\eta}\sqrt{3}/2)\ , \tag{8}$$

where (ξ,η) stand for spin up and down.

The RSO interaction couples spin-up and spin-down states, breaking the corresponding SU(2) symmetry, leading to the Hamiltonian (written in the four-component spinor Ψ basis)

$$H=\begin{pmatrix} 0 & \varphi_0 & 0 & i\varphi_+ \\ \bar{\varphi}_0 & 0 & -i\bar{\varphi}_- & 0 \\ 0 & i\varphi_- & 0 & \varphi_0 \\ -i\bar{\varphi}_+ & 0 & \bar{\varphi}_0 & 0 \end{pmatrix} \quad \Psi=\begin{pmatrix} u_{A\uparrow} \\ u_{B\uparrow} \\ u_{A\downarrow} \\ u_{B\downarrow} \end{pmatrix}, \tag{9}$$

where

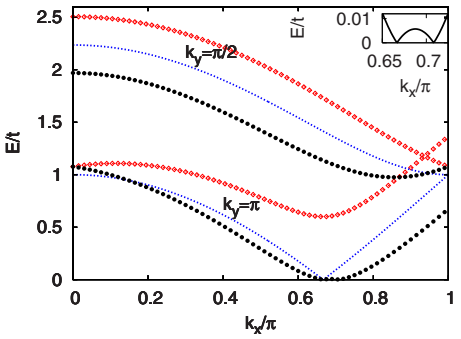

FIG. 2. (Color online) Energy bands as function of k_x of an infinite graphene plane without (small dotted lines) and with (filled circles and empty diamonds) RSO. The strength of the RSO interaction is $\lambda_R=0.2t$. The plotted bands correspond to $k_y=\pi$ (lower set) and $k_y=\pi/2$ (upper set). The inset shows the lower energy band with $k_y=\pi$ and the additional Dirac points. A finite gap separates other conduction and valence bands.

$$\varphi_0 = te^{i2k_yb/3}[1+2e^{-ik_yb}\cos(k_xa/2)],$$

$$\varphi_+ = \lambda_R e^{i2k_yb/3}[1+2\cos(k_xa/2+2\pi/3)e^{-ik_yb}],$$

$$\varphi_- = \lambda_R e^{i2k_yb/3}[1+2\cos(k_xa/2-2\pi/3)e^{-ik_yb}]. \quad (10)$$

The eigenvalue equation is given by

$$E_+^2E_-^2 = \Phi\bar{\Phi} \quad (11)$$

in which we have defined

$$E_\pm^2 = E^2-\varepsilon_0^2-\varepsilon_\pm^2,$$

$$\Phi = i\varphi_+\bar{\varphi}-i\varphi\bar{\varphi}_- = E^+E^-e^{i\nu}, \quad (12)$$

and $\varepsilon_{0;\pm}=|\varphi_{0;\pm}|$. The angle ν is defined by

$$\tan\nu = \Im\Phi/\Re\Phi. \quad (13)$$

Note that ν is *independent* of the RSO coupling.

Equation (12) shows explicitly that $E\to -E$, representing the particle-hole symmetry, is preserved by the RSO interaction. Using this property, in the rest of the paper we will focus on conduction bands only.

In Figs. 2 and 3 we plot few bands for the infinite graphene plane in the presence of the RSO interaction. Two new features appear: (a) due to the breaking of the SU(2) symmetry, each of the degenerate bands (in the absence of spin-orbit interaction) splits into two. For a given (k_x,k_y) the energies of the newly separated upper (E_u) and lower bands (E_l) are related by $E_u^2-\varepsilon_0^2-\varepsilon_\pm^2=-(E_l^2-\varepsilon_0^2-\varepsilon_\mp^2)$. (b) The inset of Fig. 2 shows the change in the band with $k_y=\pi$ which originally touches the corresponding valence band at a Dirac point located at $K=(2\pi/3a,\pi/b)$.

A remarkable consequence of the RSO interactions is the splitting of the original Dirac point caused by crossings of conduction and valence bands. The location of the new points in reciprocal space respects the underlying honeycomb symmetry and depends on the strength of the interaction λ_R as shown in Fig. 4. For the Dirac point at $K=(2\pi/3;\pi/b)$ shown in Fig. 2, the position of one new point is at $(k_x',\pi/b)$ with k_x' given by

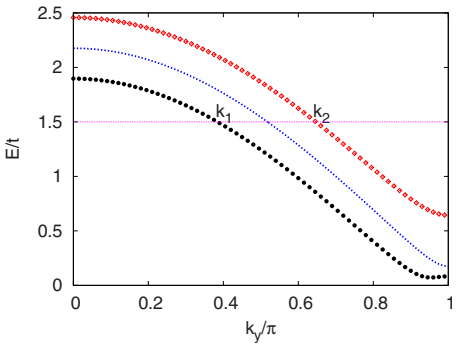

FIG. 3. (Color online) Energy bands as function of k_y of an infinite graphene plane without (small dotted lines) and with (filled circles and empty diamonds) RSO. The strength of the RSO interaction is $\lambda_R=0.2t$. The plotted bands correspond to $k_x=0.6\pi$. As described in the text there are four degenerate states at $k_y=\pm k_1$ and $k_y=\pm k_2$ for each k_x value.

$$\cos(k_x'/2) = \frac{1}{2}\frac{t^2-2\lambda_R^2}{t^2+\lambda_R^2}. \quad (14)$$

In the linear (Dirac) approximation of the Hamiltonian and for small values of the interaction strength λ_R, the splitting of the Dirac points is missed, and the low-energy effective Hamiltonian describes graphene with RSO interactions as a zero-gap semiconductor as reported in previous works.[9]

It is important to remark that the RSO interaction does not open a gap in the spectrum at the Dirac point, in contrast to the I-SO interaction mentioned above.

To solve for the eigenstates of Hamiltonian (9) we notice first that in the limit $\lambda_R\to 0$ the spinor introduced in Eq. (9) takes the form $\Psi=e^{i\nu/2}\psi_\uparrow+e^{-i\nu/2}\psi_\downarrow$, where $\psi_{\uparrow\downarrow}$ are the two degenerate spinors defined in the absence of the RSO interaction. The four components of Ψ satisfy the following relations:

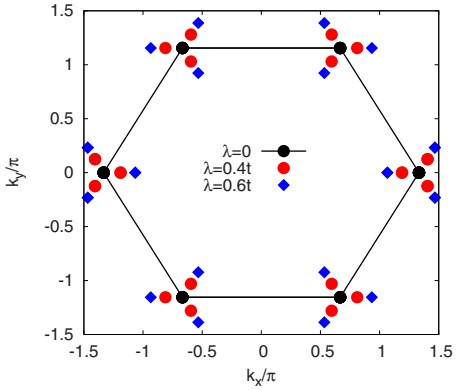

FIG. 4. (Color online) The positions of zero-energy (Dirac) points in momentum space for different values of the RSO interaction strength λ_R. The distribution of the Dirac points around the original ones has the $2\pi/3$ rotational symmetry of the graphene lattice.

$$\frac{u_{A\uparrow}}{u_{A\downarrow}} = \frac{E_-}{E_+}e^{i\nu},$$

$$\frac{u_{B\uparrow}}{u_{B\downarrow}} = \frac{E_+}{E_-}e^{i\nu},$$

$$u_{B\downarrow} = \frac{\bar{\varphi}}{E}u_{A\uparrow} - i\frac{\bar{\varphi}_-}{E}u_{A\uparrow}, \tag{15}$$

which lead to the eigenstates

$$\Psi = \begin{pmatrix} u_{A\uparrow} \\ u_{B\uparrow} \\ u_{A\downarrow} \\ u_{B\downarrow} \end{pmatrix} = \begin{pmatrix} e^{i\nu/2}\begin{pmatrix} \sqrt{\frac{E^-}{E^+}}e^{i\alpha/2} \\ \sqrt{\frac{E^+}{E^-}}e^{-i\alpha/2} \end{pmatrix} \\ e^{-i\nu/2}\begin{pmatrix} \sqrt{\frac{E^+}{E^-}}e^{i\alpha/2} \\ \sqrt{\frac{E^-}{E^+}}e^{-i\alpha/2} \end{pmatrix} \end{pmatrix}. \tag{16}$$

Here α is defined by

$$e^{i\alpha} = \frac{\varphi}{E}\frac{E^+}{E^-} + i\frac{\varphi_+}{E}e^{-i\nu} = \frac{\varphi}{E}\frac{E^-}{E^+} + i\frac{\varphi_-}{E}e^{i\nu}. \tag{17}$$

In the limit $\lambda_R \to 0$, $\sqrt{\frac{E^+}{E^-}} \to 1$ and $\alpha \to \alpha_0$. The expressions above [Eq. (16)] correspond to a state with energy E in the split upper band and momentum (k_x, k_y). The sate with the same momentum components in the split lower band is obtained by the replacement $\nu \to \nu + \pi$. The remaining particle-hole symmetric states (in the split valence bands) are obtained by taking $\alpha \to \alpha + \pi$.

Wave function (16) has the property of $u_{A\uparrow} = \bar{u}_{B\downarrow}$ and $u_{B\uparrow} = \bar{u}_{A\downarrow}$. This reflects that, in the presence of the SU(2) symmetry-breaking RSO interaction the probability of finding an electron in the spin-up state, i.e., $|u_{A\uparrow}|^2 + |u_{B\uparrow}|^2$ is equal to the probability of finding it in the spin-down state, i.e., $|u_{A\downarrow}|^2 + |u_{B\downarrow}|^2$. This is a direct consequence of the fact that the RSO interaction does not break time-reversal symmetry. However, as we will see below, this does not exclude the possibility of separating the spin-up- and spin-down-electron states and localizing them at different positions in the sample while preserving a zero net magnetization.

III. ZIGZAG GRAPHENE NANORIBBONS

A. Zigzag nanoribbons without Rashba spin-orbit interaction

To study the interplay between confinement and the RSO interaction we analyze the case of zigzag graphene (ZGR) nanoribbons, defined according to Fig. 5.

As standard practice the hard-wall boundary conditions are imposed by setting $u_A(y=0)=0$ on the lower border and $u_B(W-b/3)=0$ on the line located at a distance $b/3$ below the upper border.[34–38] After close inspection, however, one realizes that it is more convenient to label all the atoms alone each zigzag line with the same y coordinate. This is equivalent to work with the deformed lattice shown in the right panel of Fig. 5 and it amounts to perform a global gauge transformation $c_B(k_y) \to c_B(k_y)e^{2ik_y b/3}$ on the original Hamiltonian. It also represents a different choice of unit cell as described in Fig. 5. For symmetry reasons we also set the y axis to be in the center of the ribbon. With this choice, the hopping term φ reduces to

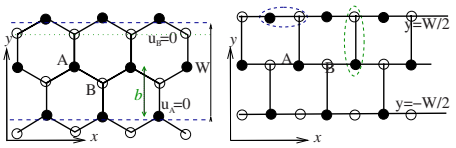

FIG. 5. (Color online) Hard-wall boundary conditions for ZGR imposes $u_A=0$ on the lower edge and $u_B=0$ just before the upper edge (dotted line). The deformed lattice shown on the right side, corresponds to a gauge transformation (see text) and it is equivalent of labeling both A and B sites in each zigzag line with the same y coordinate. The horizontal oval shows our choice of the unit cell and the vertical oval shows the choice of the unit cell which corresponds to Eq. (20).

$$\varphi(k_x, k_y) = t\left(e^{ik_y b} + 2\cos\frac{k_x a}{2}\right), \tag{18}$$

and the boundary conditions are

$$u_A(y = -W/2) = 0, \quad u_B(y = W/2) = 0. \tag{19}$$

Notice that in most of the literature on graphene ribbons the usual convention for φ and the boundary conditions are

$$u_A(y = -W/2) = 0, \quad u_B(y = W/2 - 1) = 0,$$

$$\varphi(k_x, k_y) = t\left(1 + 2\cos\frac{k_x a}{2}e^{-ik_y b}\right), \tag{20}$$

which correspond to choosing a unit cell along the vertical link in the right-side panel of Fig. 5.

The wave function of the ZGR can be found in a straightforward manner as follows. Since k_x is a good quantum number, the wave function for a given k_x must be a superposition of degenerate states with different k_y values. In the absence of SO there are only two degenerate spinors for each k_x, namely, at $k_y = k$ and $k_y = -k$. Therefore the wave function is the superposition of these two spinors: $\Psi = a\Psi(k_x, k) + b\Psi(k_x, -k)$. After applying the boundary conditions as given in Eq. (19), we find $b = -a$ such that

$$\Psi = Ne^{ik_x x}\begin{pmatrix} \sin(\alpha_0/2 + ky - n\pi/2) \\ \sin(-\alpha_0/2 + ky - n\pi/2) \end{pmatrix}, \tag{21}$$

where k satisfies

$$\alpha_0 - kW = n\pi. \tag{22}$$

Figure 6 shows the conduction bands of a ribbon with $W = 4b$. Zigzag ribbons present two remarkable features as compared to graphene sheets: the momentum across the ribbon k_y can take complex values between two Dirac points[34–38] producing edge states, and their band structure depends on the width W or the number of zigzags chains N

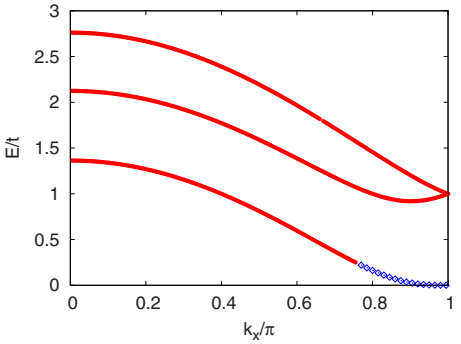

FIG. 6. (Color online) Energy bands of a zigzag ribbon with $W=4b$ in the absence of the RSO interaction. Each band is doubly degenerate due to the SU(2) spin symmetry. The edge band (diamonds) corresponds to an imaginary value for the label k in Eq. (22).

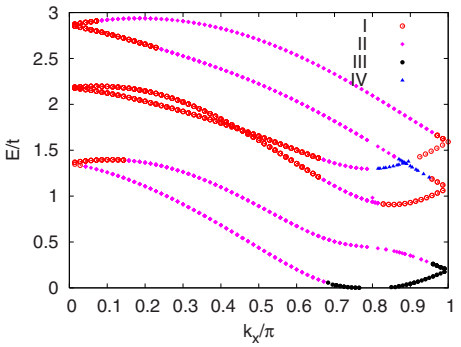

FIG. 7. (Color online) Energy bands of a ZGR with $W=4b$ and $\lambda_R=0.4t$. Different regions correspond to values of k_1 and k_2: (I) both real, (II) one real and the other one imaginary, (III) both imaginary, and (IV) complex with $k_1=k_2^*$.

$=W/b-1$. It can be shown[39–42] that in zigzag ribbons with odd number of chains N, the so-called "zigzag/zigzag" configuration, conduction, and valence edge bands cross at $k_x a=\pi$. In contrast, ribbons with even number of chains N, in the "zigzag/anti-zigzag" configuration, edge bands do not cross, albeit remain degenerate at $k_x a=\pi$.

B. Zigzag nanoribbons with Rashba spin-orbit interaction

As seen in Sec. III A, ZGRs present the peculiar feature of edge states which remain highly quasidegenerate at low energies for wide ribbons. These states are expected to be strongly affected by the presence of a RSO interaction. Below we proceed to obtain the exact expressions for the band structure and corresponding eigenstates for the ZGR with RSO interactions.

It is necessary to remark first that since the RSO interaction involves nearest-neighbor hopping, the boundary conditions as imposed in Eq. (19) remain unchanged. However, for a given value of k_x, there are four degenerate states at $k_y=\pm k_1$ and $k_y=\pm k_2$ in contrast with the previous case (with only two degenerate states at $\pm k$). This is easily seen in Fig. 3. Notice that there are certain energies, such that it seems that there are only two degenerate states; however the wave-function is really the superposition of four spinors with $\pm k_1$ and $\pm k_2$ taking imaginary or complex values. The general wave function is

$$\Psi^{\mathrm{ZGR}} = a\psi(k_1) + b\psi(-k_1) + c\psi(k_2) + d\psi(-k_2), \quad (23)$$

where $\psi(k_i)=\psi(k_x,k_i)$ and k_1 and k_2 satisfy the condition given by the degeneracy

$$E(\pm k_1) = E(\pm k_2). \quad (24)$$

Imposing the boundary conditions given in Eq. (19) yields

$$\frac{E_1^+ \sin(\mu_1^+ + \delta)}{E_1^- \sin(\mu_1^- + \delta)} = \frac{E_2^+ \sin(\mu_2^+ + \delta)}{E_2^- \sin(\mu_2^- + \delta)}, \quad (25)$$

where $\mu_i^{\mp}=(\nu_i \pm \alpha_i \mp k_i W)/2$ and $\delta=\pm\pi/2$. These two equations define the band structure and the corresponding wave function in terms of the width W and the RSO coupling λ_R. The wave-function coefficients are given by

$$a = -b = N\sqrt{\frac{E_2^-}{E_2^+}}\sin(\mu_2^+ + \delta),$$

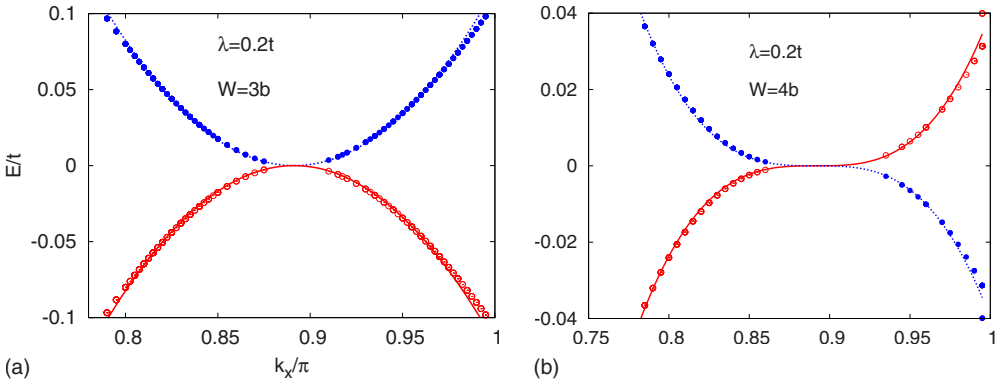

FIG. 8. (Color online) The left panel shows the edge bands of a ribbon with $W=3b(N=2)$ and $\lambda_R=0.2t$. Conduction and valence edge bands do not cross at the band center. In contrast, the right panel shows a $W=4b(N=3)$ ribbon with crossing bands. The full lines are fits using the expression in Eq. (28).

$$d = -c = N\sqrt{\frac{E_1^-}{E_1^+}}\sin(\mu_1^+ + \delta), \tag{26}$$

where N is the normalization factor. From these expressions it can be shown that $\Psi_{A\uparrow}^{\mathrm{ZGR}}(y) = i\Psi_{B\downarrow}^{\mathrm{ZGR}}(-y)$ and $\Psi_{A\downarrow}^{\mathrm{ZGR}}(y) = i\Psi_{B\uparrow}^{\mathrm{ZGR}}(-y)$.

Figure 7 shows the conduction bands for a ribbon with $W=4b$ and $\lambda_R=0.4t$. Starting at $k_x=0$ both parameters k_1, k_2 are real (region I). As k_x is increased, k_2 goes to π or zero and in region II it becomes complex (with constant real part equal to π) or purely imaginary. In region III both k_1 and k_2 take imaginary values with a constant real part of π or zero. The energy of the lower band goes to zero $E=0$ at the point k_x^0 defined by

$$\cos\left(\frac{k_x^0 a}{2}\right) = \sqrt{\frac{3\lambda_R^2}{4\lambda_R^2 + 4t^2}}. \tag{27}$$

Notice finally that there is also a region (IV) where k_1 and k_2 are complex conjugate of each other. As it occurs with the I-SO interaction, the presence of the RSO interaction lifts the apparent quasidegeneracy of the edge band while preserving the Dirac points.[12] The expression for the dispersion of the edge bands of an N-wide ribbon is readily obtained and is given by

$$E \approx \pm t(k_x a - k_x^0 a)^N, \tag{28}$$

where k_x^0 is defined in Eq. (27). It is interesting to notice that RSO interactions preserve the power law energy dispersion and edge bands crossing/anticrossing feature as shown in Figs. 8.

With the expressions obtained for the wave functions, it is possible to calculate various quantities. In particular, Fig. 9 shows the spatial probability distribution for S^z, the z component of the spin operator defined as $\langle S^z\rangle = |u_{A\uparrow}|^2 + |u_{B\uparrow}|^2 - |u_{A\downarrow}|^2 - |u_{B\downarrow}|^2$ for the lowest-energy conduction band of a ribbon with $W=4b$ and $\lambda_R=0.4t$.

The figure highlights the fact that the RSO interaction produces a clear spin polarization on the edge states of the ZGR. The nonhomogeneous spin distribution across the ribbon is, however, highly dependent on the state considered. This is in contrast to the effect produced by the I-SO interaction where each state becomes spin-polarized with the same spatial spin distribution.[12]

IV. CONCLUSIONS

Graphene ribbons show unique and interesting transmission properties due to its band-structure and the pseudo-spin nature of its wave functions.[39,40] The relativistic nature of the description normally used makes it necessary to understand further other relativistic effects that could alter their transport properties. In this work we have investigated the consequences of one of such interactions: the Rashba spin-orbit interaction that is expected to be relevant under applied external bias voltages. We have shown that in graphene sheets, the RSO removes the SU(2) spin degeneracy as expected while it does not open a gap in the spectrum. It does, however, introduce additional Dirac points in the Fermi surface at low energies due to crossings between valence and conduction bands.

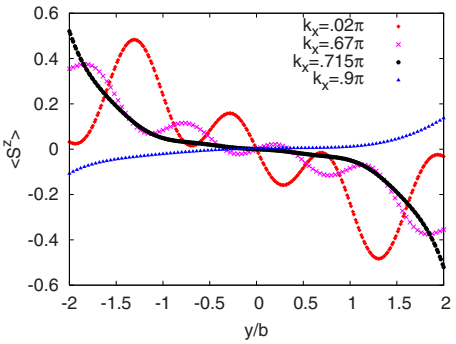

FIG. 9. (Color online) Expectation value of the z projection of the spin operator, $\langle S^z\rangle$ as a function of position across the ribbon. The curves are calculated using the lowest energy conduction band of a ZGR with $W=4b$ and $\lambda_R=0.4t$. Different curves correspond to different values of k_x of Fig. 7

Because of its peculiar edge band, zigzag graphene ribbons are potential candidates for spintronic applications. The edge bands are expected to be magnetically unstable and as such to be strongly affected by SO interactions. We have shown that the RSO in particular produces states that have spin polarization and are strongly localized along the edges. These states present opposite polarization at opposite edges and the spatial spin distribution is strongly dependent on the state under consideration. Without external fields the net spin polarization of the ribbon remains null as a natural consequence of the conservation of time-reversal symmetry under the RSO interaction. However, these results suggest the possibility to obtain spin-polarized currents if the states selected by an applied external voltage sustain an *average* nonzero spin polarization.

ACKNOWLEDGMENTS

We acknowledge S. E. Ulloa and G. Diniz for useful discussions. This work was supported by NSF under Grants No. DMR 0710581 and PHY05-51164, and by Ohio University BNNT funds.

[1] S. Murakami, Adv. Solid State Phys. **45**, 197 (2005).
[2] S. Murakami, N. Nagaosa, and S. C. Zhang, Science **301**, 1348 (2003).
[3] J. Sinova, D. Culcer, Q. Niu, N. A. Sinitsyn, T. Jungwirth, and A. H. MacDonald, Phys. Rev. Lett. **92**, 126603 (2004).
[4] M. I. Dyakonov and V. I. Perel, JETP Lett. **13**, 467 (1971).
[5] J. E. Hirsch, Phys. Rev. Lett. **83**, 1834 (1999).
[6] E. I. Rashba, Sov. Phys. Solid State **2**, 1109 (1960); Yu. A.

Bychkov and E. I. Rashba, JETP Lett. **39**, 78 (1984).
[7] K. S. Novoselov, A. K. Geim, S. V. Morozov, D. Jiang, M. I. Katsnelson, I. V. Grigorieva, S. V. Dubonos, and A. A. Firsov, Nature (London) **438**, 197 (2005); K. S. Novoselov, D. Jiang, F. Schedin, T. J. Booth, V. V. Khotkevich, S. V. Morozov, and A. K. Geim, PNAS **102**, 10451 (2004).
[8] See for example: A. H. Castro Neto, F. Guinea, N. M. R. Peres, K. S. Novoselov, and A. K. Geim, Rev. Mod. Phys. **81**, 109 (2009).
[9] C. L. Kane and E. J. Mele, Phys. Rev. Lett. **95**, 226801 (2005).
[10] C. L. Kane and E. J. Mele, Phys. Rev. Lett. **95**, 146802 (2005).
[11] M. Zarea and N. Sandler, Phys. Rev. Lett. **99**, 256804 (2007).
[12] M. Zarea, C. Büsser, and N. Sandler, Phys. Rev. Lett. **101**, 196804 (2008), and references therein.
[13] Y. W. Son, M. L. Cohen, and S. G. Louie, Phys. Rev. Lett. **97**, 216803 (2006).
[14] Y. W. Son, M. L. Cohen, and S. G. Louie, Nature (London) **444**, 347 (2006).
[15] D. A. Abanin, K. S. Novoselov, U. Zeitler, P. A. Lee, A. K. Geim, and L. S. Levitov, Phys. Rev. Lett. **98**, 196806 (2007).
[16] M. Wimmer, I. Adagideli, S. Berber, D. Tomanek, and K. Richter, Phys. Rev. Lett. **100**, 177207 (2008).
[17] Z. Jiang, Y. Zhang, H. L. Stormer, and P. Kim, Phys. Rev. Lett. **99**, 106802 (2007).
[18] B. Wunsch, T. Stauber, F. Sols, and F. Guinea, Phys. Rev. Lett. **101**, 036803 (2008).
[19] B. Huang, F. Liu, J. Wu, B. L. Gu, and W. Duan, Phys. Rev. B **77**, 153411 (2008).
[20] H. Kumazaki and D. S. Hirashima, J. Phys. Soc. Jpn. **77**, 044705 (2008).
[21] D. E. Jiang, B. G. Sumpter, and S. Dai, J. Chem. Phys. **127**, 124703 (2007).
[22] L. R. Radovic and B. Bockrath, J. Am. Chem. Soc. **127**, 5917 (2005).
[23] S. Trickey, *Lecture Notes on Electronic States and Excitation on Nanostructures* (PASI School, Zacatecas, Mexico, 2007).
[24] J. C. Boettger and S. B. Trickey, Phys. Rev. B **75**, 121402(R) (2007).
[25] H. Min, J. E. Hill, N. A. Sinitsyn, B. R. Sahu, L. Kleinman, and A. H. MacDonald, Phys. Rev. B **74**, 165310 (2006).
[26] D. Huertas-Hernando, F. Guinea, and A. Brataas, Phys. Rev. B **74**, 155426 (2006).
[27] Yu. S. Dedkov, M. Fonin, U. Rudiger, and C. Laubschat, Phys. Rev. Lett. **100**, 107602 (2008).
[28] N. Tombros, C. Jozsa, M. Popinciuc, H. T. Jonkman, and B. J. van Wees, Nature (London) **448**, 571 (2007).
[29] N. Tombros, S. Tanabe, A. Veligura, C. Jozsa, M. Popinciuc, H. T. Jonkman, and B. J. van Wees, Phys. Rev. Lett. **101**, 046601 (2008).
[30] D. Huertas-Hernando, F. Guinea, A. Brataas, arXiv:0812.1921 (unpublished).
[31] A. Varykhalov, J. Sanchez-Barriga, A. M. Shikin, C. Biswas, E. Vescovo, A. Rybkin, D. Marchenko, and O. Rader, Phys. Rev. Lett. **101**, 157601 (2008).
[32] A. De Martino, R. Egger, K. Hallberg, and C. A. Balseiro, Phys. Rev. Lett. **88**, 206402 (2002).
[33] Y. Yao, F. Ye, X.-L. Qi, S.-C. Zhang and Z. Fang, Phys. Rev. B **75**, 041401(R) (2007).
[34] M. Fujita, J. Phys. Soc. Jpn. **65**, 1920 (1996).
[35] K. Nakada, M. Fujita, G. Dresselhaus, and M. S. Dresselhaus, Phys. Rev. B **54**, 17954 (1996).
[36] L. Brey and H. A. Fertig, Phys. Rev. B **73**, 235411 (2006).
[37] T. Hikihara, X. Hu, H.-H. Lin, and C.-Y. Mou, Phys. Rev. B **68**, 035432 (2003).
[38] A. R. Akhmerov and C. W. J. Beenakker, Phys. Rev. B **77**, 085423 (2008).
[39] A. Rycerz, J. Tworzydlo, and C. W. J. Beenakker, Nat. Phys. **3**, 172 (2007).
[40] A. R. Akhmerov, J. H. Bardarson, A. Rycerz, and C. W. J. Beenakker, Phys. Rev. B **77**, 205416 (2008).
[41] Z. Li, H. Qian, J. Wu, B.-L. Gu, and W. Duan, Phys. Rev. Lett. **100**, 206802 (2008).
[42] M. Zarea and N. Sandler (unpublished).